

Development of Immobilized SPINOL-Derived Chiral Phosphoric Acids for Catalytic Continuous Flow Processes. Use in the Catalytic Desymmetrization of 3,3-Disubstituted Oxetanes

Junshan Lai, Mauro Fianchini, and Miquel A. Pericàs*

ABSTRACT: A family of C_2 -symmetrical 1,1'-spirobiindane-7,7'-diol (SPINOL) derivatives containing polymerizable styryl units has been prepared through a highly convergent approach. Radical co-polymerization of these monomers with styrene has allowed the synthesis of a family of immobilized SPINOL-derived chiral phosphoric acids (SPAs) where the combination of the restricted axial flexibility of the SPINOL units and the existence of extended and adaptable chiral walls adjacent to them leads to enhanced stereocontrol in catalytic processes. The optimal immobilized species (**Cat f**) brings about the catalytic desymmetrization of 3,3-disubstituted oxetanes in up to 90% yield with up to >99% enantioselectivity, exhibiting a very high recyclability (no decrease in conversion or enantioselectivity after sixteen, 16-hour runs). To exploit these characteristics, a continuous flow process has been implemented and operated for the sequential preparation of 17 diverse enantioenriched products. The suitability of the flow setup for gram scale preparations (20 mmol scale), the stability of **Cat f** for long periods of time with intermittent use in flow, and its deactivation/reactivation by treatment with pyridine/hydrochloric acid in dioxane have been demonstrated. Density Functional Theory has been employed to provide a rational justification of the deep effect on enantioselectivity arising from the presence of sterically bulky substituents at the 6,6'-positions of the SPINOL unit. The main structural features of **Cat f** have subsequently been incorporated to the design of a simplified homogeneous analog available in a straightforward manner (**Cat g**) that performs the benchmark desymmetrization reaction with similar yields and enantioselectivities as **Cat f**, providing a convenient alternative for cases when single use in solution is sought.

KEYWORDS: Chiral Phosphoric Acids • Immobilization • SPINOL • Continuous Flow • Density Functional Theory.

Among the different families of successful organocatalysts, chiral phosphoric acids stands out for the unique peculiarity of combining a Lewis basic site with a Brønsted acid site within the same catalytic unit.¹⁻⁵ Moreover, since the first pioneering works of Akiyama,⁶ Terada and Uraguchi⁷ in 2004, the high versatility of BINOL-derived chiral phosphoric acids (BPAs) as Brønsted acid-Lewis base catalysts translates in over 500 publications.^{2-4, 6-20} Drawbacks in the use of BPAs in asymmetric catalysis can be ascribed to the conformational flexibility of the BINOL scaffold that may hamper enantioselection,²¹ or to the unaffordable cost in derivatives like TRIP, where this problem has been solved through the introduction of very bulky substituents in the 2,2' positions.¹² A conceptual, synthetic evolution of BINOL, 1,1'-spirobiindane-7,7'-diol or SPINOL (**1**), first introduced by Birman in 1999,²² and its derivatives found initial application as ligands in asymmetric metal catalysis.²³⁻²⁴ From 2010 on, a new generation of SPINOL-derived phosphoric acids (SPAs) has been developed.²⁵⁻²⁶ Over the last decade, both the number of synthetic procedures for the preparation of SPAs and their catalytic applications have sensibly grown, leading to the characterization of diverse chiral SPAs and their application in different catalytic processes resulting in over 100 publications.²⁷ The most significant advantage of SPAs over BPAs lays in the structural rigidity of the C_2 -symmetric chiral spirocyclic backbone: the configuration of the quaternary carbon in SPINOLS is blocked. Thus, conformational mobility is completely restricted and racemization in solution becomes virtually impossible. Thus, the chemical robustness and conformational rigidity of SPAs enables different electronic and steric factors compared to those of BPAs. Following pioneering work by Birman,²² a considerable amount of work involving the use in catalysis of structures with spirocyclic backbones has been reported.^{24, 28-36} Thus, asymmetric syntheses of SPINOL and SPIROL derivatives (**2-5**) have been achieved by the Tan,³⁰ Ding,^{29,35} Nagorny,³⁴ and Lu/Hayashi/Dou groups³⁶ (Figure 1).

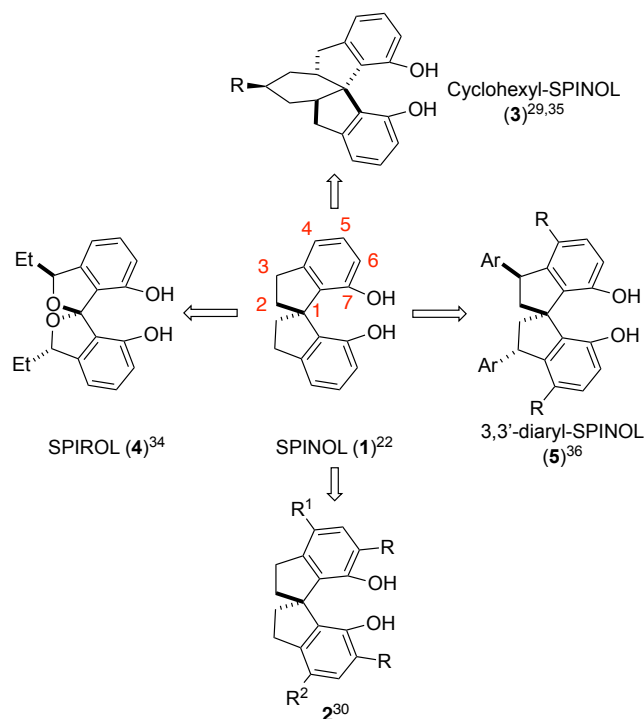


Figure 1. Development of SPINOL and SPIROL derivatives.

Most notably, Lu, Hayashi, Dou and coworkers reported in 2019 a highly diastereo- and enantioselective synthesis of 3,3'-diaryl-SPINOLS (**5**) and could show that the derived phosphoramidite ligands showcased higher enantioselectivities than those containing the non-substituted SPINOL skeleton in several different types of catalytic asymmetric processes.³⁶ In addition, it has been shown²⁷ that bulky substituents at the 6,6'-positions on the SPINOL skeleton in derived phosphoric acids are essential for the achievement of optimal enantiocontrol with

SPINOL-derived ligands and organocatalysts. This is not a trivial detail, since the introduction of such substituents always requires additional synthetic steps leading to increased production costs that could hamper large scale application. This limitation, however, could be efficiently mitigated by immobilization of the catalyst onto solid supports. If correctly planned, this strategy could allow the easy recovery and recycling of the catalyst (thus extending its useful life span) and easy product isolation without paying a penalty in catalytic activity.^{37,38} Moreover, catalytic processes based on immobilized catalysts often present the remarkable advantage of allowing implementation in continuous-flow.³⁹⁻⁵⁶ As a consequence of these advantages, interest in the immobilization of homogeneous chiral catalysts onto diverse solid supports has spread in recent years,⁵⁷⁻⁶¹ chiral phosphoric acids clearly illustrating this tendency.

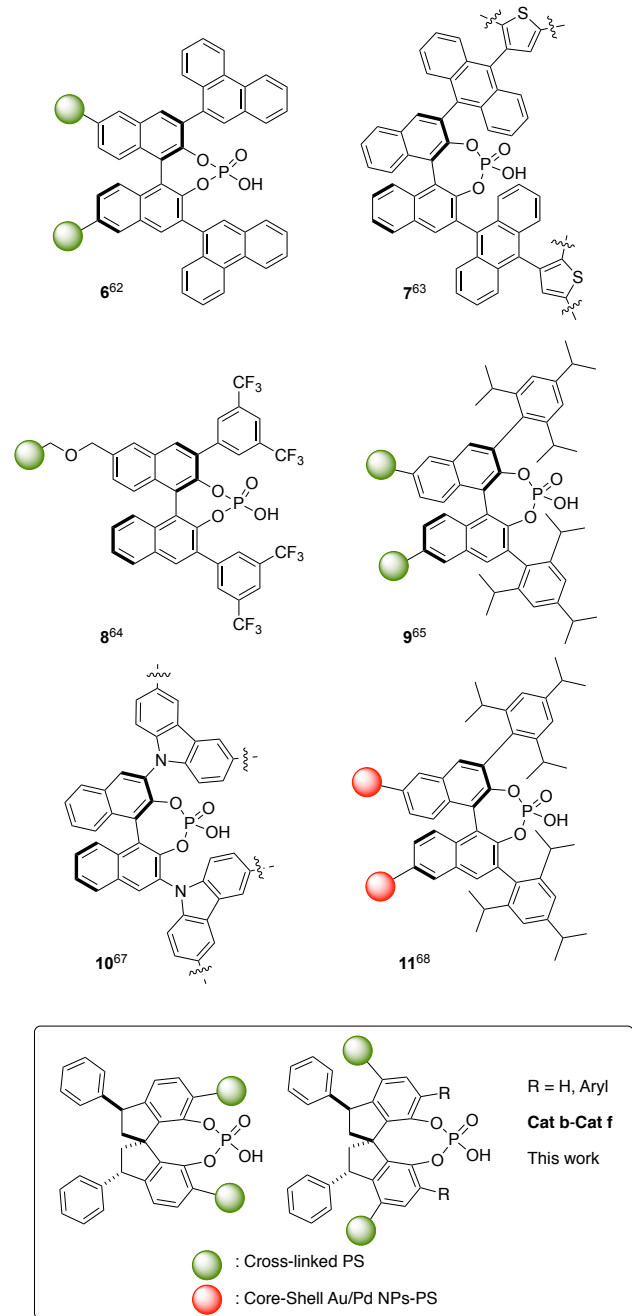


Figure 2. Immobilized chiral phosphoric acids.

Thus, Rueping⁶² and Blechert⁶³ already envisioned the potential advantages of immobilization of chiral phosphoric acids onto

stationary phases (Structures 6 and 7 in Figure 2). Later on, the Pericàs laboratory developed immobilized CPAs 8 and 9 and demonstrated their practicality for long-time operable, highly enantioselective processes in continuous flow.⁶⁴⁻⁶⁶ Structures 10 and 11 correspond to more recent developments exemplifying the continued interest for the immobilization of CPAs.^{67,68} We report in this manuscript the synthesis of a family of 3,3'-diphenyl-SPINOL bearing polymerizable substituents at either C4-C4' or C6-C6', their immobilization by copolymerization, the preparation of the corresponding CPAs (**Cat b-Cat f**) and the use of these catalytic species for the desymmetrization of 3-substituted oxetanes with benzothiazole thiols (up to 90% yield and >99% ee) has been tested both in batch and in flow. These experimental studies are complemented by a theoretical (DFT) analysis of the factors governing the enantioselectivity of the desymmetrization process that opens new perspectives for the design of even more efficient catalysts of this type. Finally, a minimalistic homogeneous analog (**Cat g**) incorporating the key elements suggested by the DFT study has been prepared and evaluated.

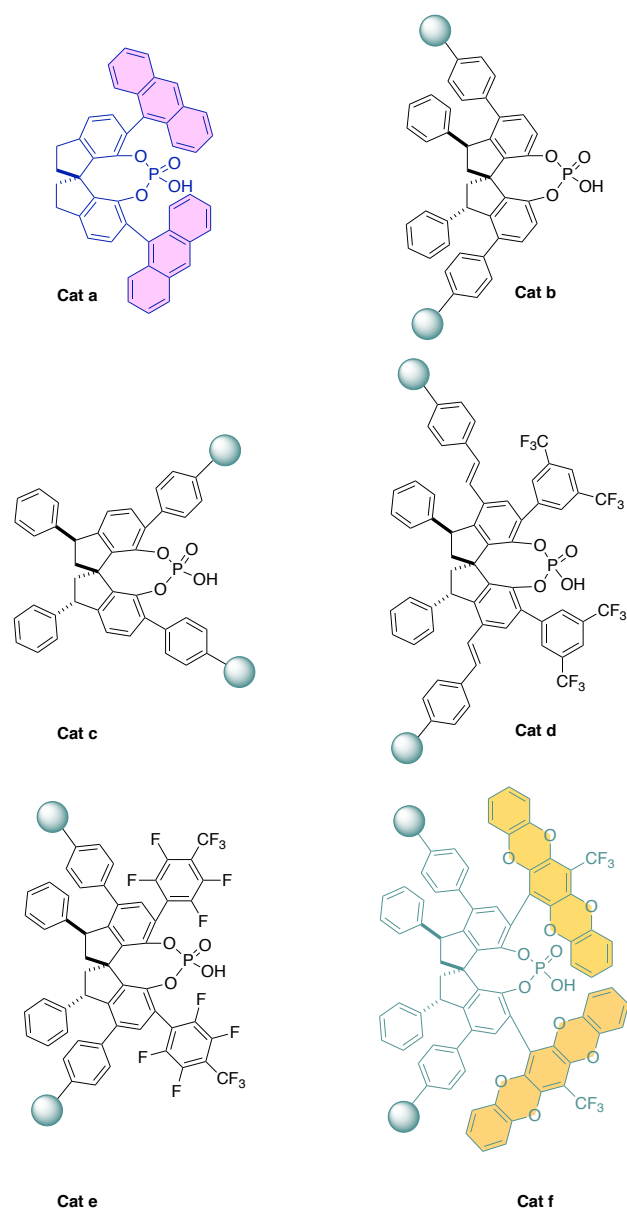


Figure 3. Immobilized SPINOL-derived chiral phosphoric acids prepared in this study.

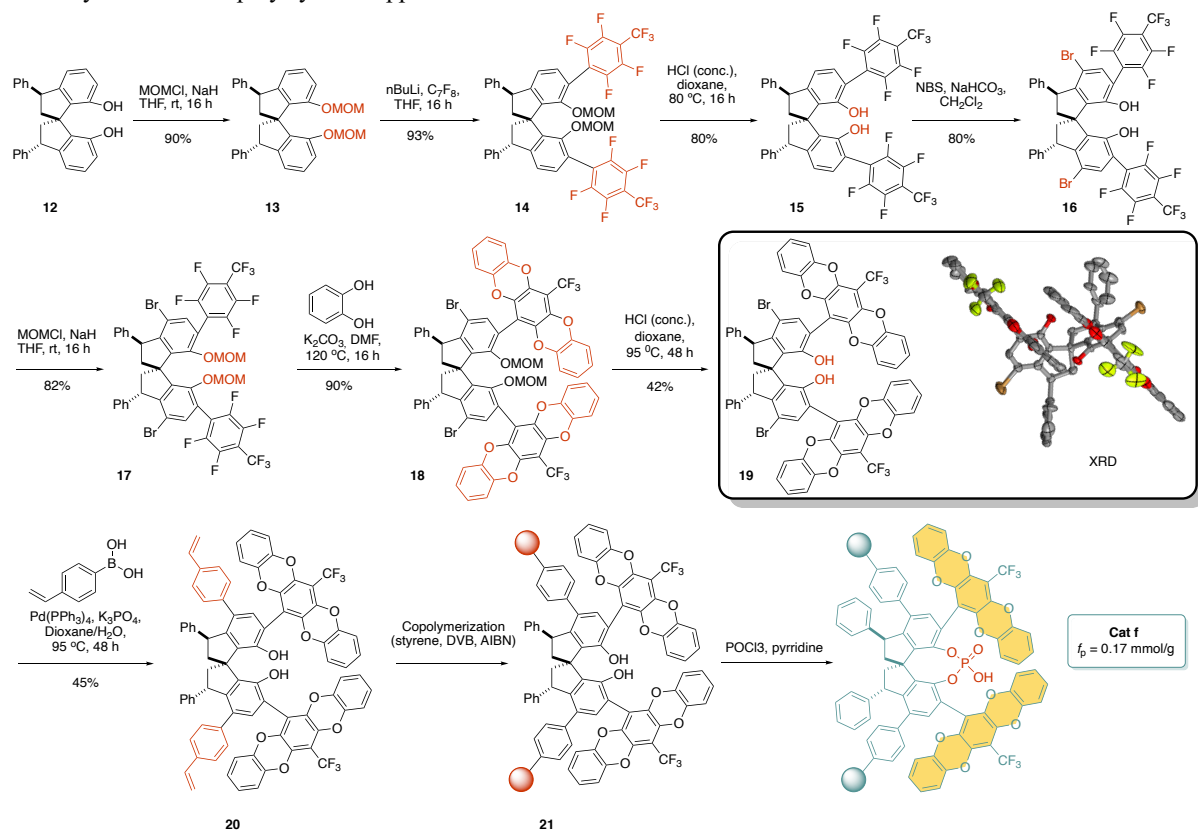
For comparison purposes, we designate the homogeneous 6,6'-bis(9-anthryl) SPA as **Cat a** (Figure 3). We will discuss here the preparation of **Cat f** as a most representative example of our modular approach to these catalytic species (Scheme 1). On the other hand, full details for the preparation of **Cat b-Cat e** can be found in the Supporting Information.

For the preparation of polystyrene immobilized SPAs (**Cat b-Cat f**) in high enantiomeric purity, the method of Lu, Hayashi and Dou was used as an efficient entry to the key SPINOL intermediates **12**, **S1** and **S4**.³⁶ Diol **12** can be sequentially functionalized at 6,6' and 4,4'. Functionalization at 6,6' was used for the introduction of specific substituents, in order to improve enantioselectivity control (in **Cat e** and **Cat f**), or to introduce a polymerizable styryl substituent (in **Cat c**). Alternatively, SPINOLs **S1** and **S4**, possessing innate bromo substituents at 4,4' and 6,6', were used to access **Cat b** and **Cat d**, respectively. Except for **Cat d**, all the prepared immobilized species are bonded to the polymer backbones through p-phenylene linkers. In the case of **Cat d**, easy diformylation at 4,4' by means of a Duff reaction dictated a Wittig strategy for the generation of a *p*-styrylene linker.

The starting material for the preparation of **Cat f**, 3,3'-diphenylSPINOL (**12**) was prepared in multigram amount with high enantiomeric purity (>99% ee) as a single diastereomer following the reported procedure.³⁶ To direct the introduction of 6,6' aryl substituents, the phenolic units were first protected as MOM ethers (**13**, 90% yield). Then, double *ortho* lithiation (*n*-BuLi, THF, 0 °C to rt) followed by treatment with perfluorotoluene at -78 °C, selectively led to the 6,6'-bis(arylated) product **14** in 93% yield.⁶⁹ The standard deprotection of the MOM ethers in **14** (HCl in dioxane), followed by regioselective dibromination at 4,4' with NBS in dichloromethane afforded **16** in 64% yield (2 steps). At this stage, the phenolic units were re-

protected as MOM ethers (**17**, 82% yield), and the protected intermediate was reacted with catechol in the presence of K₂CO₃ to increase the structural complexity of the aryl substituents at 6,6' (**18**, 90% yield).⁷⁰ The deprotection of the MOM ethers in **18** required rather harsh conditions, diol **19** being obtained in 42% yield. Interestingly, monocrystals of **19** could be grown from a mixture of iodobenzene and hexane. X-ray diffraction (see Supporting Information) confirmed the structure and configuration of the compound, showing two molecules of **19** per unit cell that display π - π stacking between the heteroaromatic wings at the 6,6' positions, with interplane distances of 3.5-3.6 Å. As discussed below, the logic of the transformation leading to the pentacyclic substituents in 6,6' was precisely that of creating a deep chiral groove around the active phosphoric acid site that will favor enantiocontrol in catalytic processes mediated by **Cat f**. It is also worth mentioning here that the apparently antieconomic protection/deprotection sequences of the phenolic units are necessary for: a) the selective introduction of the perfluoroaryl substituents at 6,6'; b) the subsequent bromination at 4,4'; c) the aromatic nucleophilic substitutions leading to the formation of the pentacyclic substituents at 6,6' and d) the ultimate Suzuki coupling with 4-vinylphenylboronic acid in the presence tetrakis(triphenylphino)palladium (0) leading to the introduction of the polymerizable units in **20** (19% yield, two steps). Unfortunately, attempts to improve the yield of the Suzuki coupling with the use of Pd₂(dba)₃/S-Phos proved unsuccessful. The polystyrene-supported SPINOL **21** was then prepared by copolymerization with styrene and DVB induced by AIBN, and **Cat f** was generated by reaction of **21** with POCl₃. The functionalization of the polymer was determined by phosphorus elemental analysis providing a value of $f_p = 0.17$ mmol/g, very appropriate for catalytic purposes.

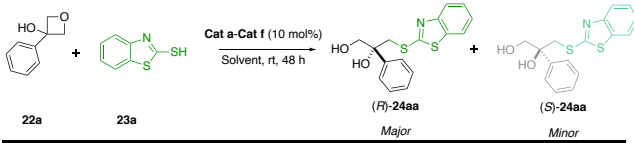
Scheme 1. Synthesis of the polystyrene-supported SPA **Cat f**.



From a practical perspective, it is important to highlight that the preparation of **19** can be significantly shortened by obviating the isolation of some of their precursors. Thus, **16** can be advantageously prepared from **14** in 70% yield (two steps), while **19** can be reached from **16** in 59% yield (three steps). In this manner, the overall yield for the preparation of **19** from **12** more than doubles from 16.6% in the step-by-step procedure to 34.5% in the optimized one, while three chromatographic purifications are avoided.

As a benchmark of the catalytic performance of the PS-supported SPAs **Cat b-Cat f**, we selected the desymmetrization of 3,3-disubstituted oxetanes. This scaffold is increasingly used in drug design,⁷¹ and the desymmetrizing ring-opening of these chiral structures could be relevant to their use as prodrugs. The reaction of 3-phenyloxetan-3-ol (**22a**) with benzo[d]thiazole-2-thiol (**23a**) was used for the selection of the optimal immobilized catalytic species and for solvent optimization (Table 1). It is to be mentioned that this reaction had been previously studied by Sun and coworkers with homogeneous CPAs as catalysts,⁷² 6,6'-bis(9-anthryl) SPA providing in that case the best results in terms of yield and enantioselectivity. As already mentioned, we have now used this compound (designated as **Cat a**) as a reference for the immobilized species.

Table 1. Catalyst and solvent optimization in the desymmetrization of **22a** with **23a** mediated by **Cat a-Cat f**.^a



Entry	Solvent	Catalyst	Yield [%]	ee [%]
1 ⁷²	CH ₂ Cl ₂	Cat a	91	97
2	CH ₂ Cl ₂	Cat b	85	20
3	CH ₂ Cl ₂	Cat c	85	63
4	CH ₂ Cl ₂	Cat d	87	72
5	CH ₂ Cl ₂	Cat e	90	83
6	CH ₂ Cl ₂	Cat f	81	90
7	toluene	Cat e	92	76
8	Et ₂ O	Cat e	90	81
9	1,2-DCE	Cat e	90	82
10	CHCl ₃	Cat e	90	86
11	CHCl ₃ /toluene (1:9)	Cat e	86	86
12	CHCl ₃	Cat f	92	95
13	CHCl ₃ /toluene (1:9)	Cat f	88	87
14 ^b	CHCl ₃	Cat f	92	98
15 ^{b,c,d}	CHCl ₃	Cat f	95	97
16 ^{b,c,d,e}	CHCl ₃	Cat f	90	97

^aStandard conditions: **22a** (30 mg, 0.2 mmol), **23a** (42 mg, 0.25 mmol), **Cat a-f** (10 mol%); for the immobilized SPAs, calculated according to the determined functionalization) in the specified solvent (1 mL), shaking at room temperature for 48 h. Under these conditions, **23a** is only partially soluble. ^bReaction under more dilute conditions (4 mL CHCl₃) to favor solubility of **23a**. ^cReaction

performed at 60 °C. ^dReaction time was 16 h (overnight). ^e5 mol% catalyst was used.

For the initial screening, the reaction of **22a** with **23a** was performed in dichloromethane in the presence of **Cat b-Cat f** and compared with the results reported for **Cat a** under identical conditions (entries 1-6). Although yields were satisfactory in all cases, it became clear from these results that a combination of bulky substituents at 6,6' and rotational mobility of these substituents was required for high enantioselectivity (entries 2 and 3). Thus, **Cat c**, in spite heavy substitution at 6,6' (the polymer backbone), did not behave as an efficient catalyst from the perspective of enantiocontrol, probably because of the lack of flexibility of this critical region of the molecule. This result directed our interest towards the catalysts immobilized through the 4,4' positions. Among them, the most promising results were those achieved with **Cat e** and **Cat f** (entries 5 and 6), while the increased conformational adaptability of the catalytic units with respect to the polymer backbone that could be present in **Cat d** thanks to the *p*-styrylene linker does not appear to play any significant positive effect (entry 4). For this reason, special attention was paid to the optimization of reaction conditions with these two ligands.

It is important to point out that, from a chronological perspective, **Cat e** was designed and prepared first, with the aim of exploring the combination of steric and electronic effects by the perfluoroaryl substituents at 6,6' on enantioselectivity, already pointed out by **Cat d** (entry 4). At a later stage in the project, the susceptibility of those perfluoroaryl substituents towards nucleophilic aromatic substitution was used as a vehicle for the preparation of **Cat f** where, as discussed below, the pentacyclic heteroaryl substituents at 6,6' play a fundamental role on the catalytic performance.

The use of **Cat e** in combination with different solvents was studied in detail. The use of more benign solvents (THF, 2-methyltetrahydrofuran, ethyl acetate, acetone, 1,4-dioxane, methanol) was studied first, but none of these solvents led to measurable conversion in the studied process. When using toluene, diethyl ether or 1,2-dichloroethane (entries 7-9) the results were similar to those achieved with dichloromethane, and only with the use of chloroform (entry 10) some improvement in enantioselectivity (86%) was noticed. Interestingly, very similar results were recorded when a 9:1 mixture of toluene and chloroform was used as the solvent (entry 11).

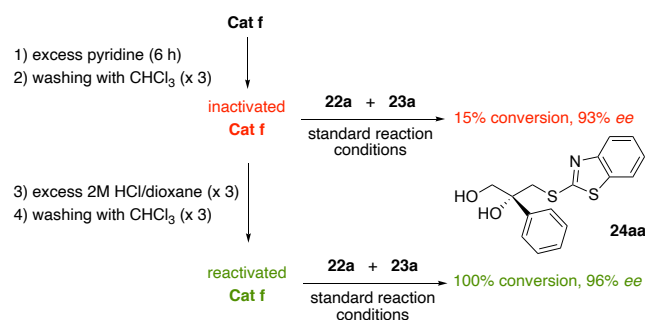
When **Cat f** was used (entries 12, 14-16) in chloroform, yield and enantioselectivity even outperformed those recorded with the homogeneous reference **Cat a**. Thus, with 0.05M initial concentration of **22a**, enantioselectivity achieved 98% (entry 14). Interestingly, the reaction time in CHCl₃ could be significantly shortened by performing the reaction at 60 °C, the reaction being completed overnight under these conditions (entry 15), and the catalyst loading could be decreased to 5 mol% without decrease in enantioselectivity (entry 16). On the other hand, with **Cat f** the use of 9:1 mixture of toluene and chloroform had a negative effect on the performance of the reaction (entry 13), so that advantages derived from the use of this more benign solvent are counterbalanced by a significant decrease in enantioselectivity.

Once we had established that **Cat f** exhibited optimal characteristics in the target desymmetrization of **22a** with thiol **23a**, we next studied the recyclability of this catalyst under the most productive conditions (those of entry 16 in Table 1). In this manner, sixteen consecutive cycles of sixteen hours could be

run without substantial loss of yield and enantioselectivity. After each cycle the resin was simply separated by filtration and immediately reused in the next reaction cycle. Table S1 shows that there are negligible fluctuations in the results obtained for yields and enantioselectivity between the 1th and the 16th reaction cycles. The cumulative turnover number (TON) achieved in these sixteen runs was 280.

Previous experience in our laboratory with immobilized CPAs has shown that the only significant deactivation mode is deprotonation by basic components in reaction mixtures. Fortunately, this is a reversible process and previously studied immobilized CPAs have shown to be easily reactivated by treatment with acid.^{64,65} Although **Cat f** did not show any sign of deactivation during the recycling experiment, we decided to force the base-induced deactivation of the catalyst to confirm the possibility of a subsequent reactivation. To this end (Scheme 2), a sample of **Cat f** was deactivated by treatment with excess pyridine for 6 h. Then, the use of this deactivated catalyst in the reaction of **22a** with **23a** under the standard conditions of Table 1 led to only 15% conversion, although enantioselectivity kept high (93%). Interestingly, the employed catalyst sample could be reactivated by treatment with 2M HCl in dioxane and reused in the reaction after washing with chloroform. In this manner, complete conversion of **22a** and 96% enantioselectivity in the formation of **24aa** were recorded.

Scheme 2. Deactivation/reactivation of the polystyrene-supported SPA **Cat f**.



In view of the excellent recyclability depicted by **Cat f** and its compatibility with rather high temperatures, with the derived consequence of short reaction times, we decided to explore the desymmetrization as a genuine flow process, bypassing any intermediate scope development in batch. For the flow experiments, 2.0 g of **Cat f** ($f = 0.17$ mmol/g, 0.34 mmol) were loaded in a size adjustable, jacketed tubular reactor. The feed of the reactor could be selected through a three-way valve from the appropriate mixture of **22** and **23** (they are unreactive to one another in the absence of **Cat f**) to the reaction solvent (chloroform) for resin cleaning between distinct operations. At the reactor outlet, a back-pressure regulator was intercalated to secure uneventful operation near the boiling point of chloroform (Figure 4)

As an initial step, the parameters of reaction temperature, concentration of **22a**, and combined flow rate were optimized for the simultaneous achievement of high yield and enantioselectivity in the reaction with **23a** leading to **24aa**. Full data for the optimization process can be found in the Supporting Information (Table S3). In summary, work at 60 °C is highly recommended for high yield with no penalty in enantioselectivity, and two sets of [**22a**]/flow rate conditions seem to be equally suitable:

a) Work with 0.05 M **22a** in chloroform at 1 mL/min (residence time = 8 min) leads to a conversion of 92% and enantioselectivity of 97%, and b) Work with 0.1 M **22a** in chloroform at 0.5 mL/min (residence time = 15 min) leads to a conversion of 98% and enantioselectivity of 95%. In all these experiments, a 25 mol% excess of **23a** was used. As a general comment, the productivity of the experiments under any of the two optimal sets of experimental conditions is remarkable (*ca.* 8 mmol_{24aa}·mmol_{Cat f}⁻¹·hour⁻¹) and can be further increased till *ca.* 14 mmol_{24aa}·mmol_{Cat f}⁻¹·hour⁻¹ at the expense of a somewhat lower instant conversion.

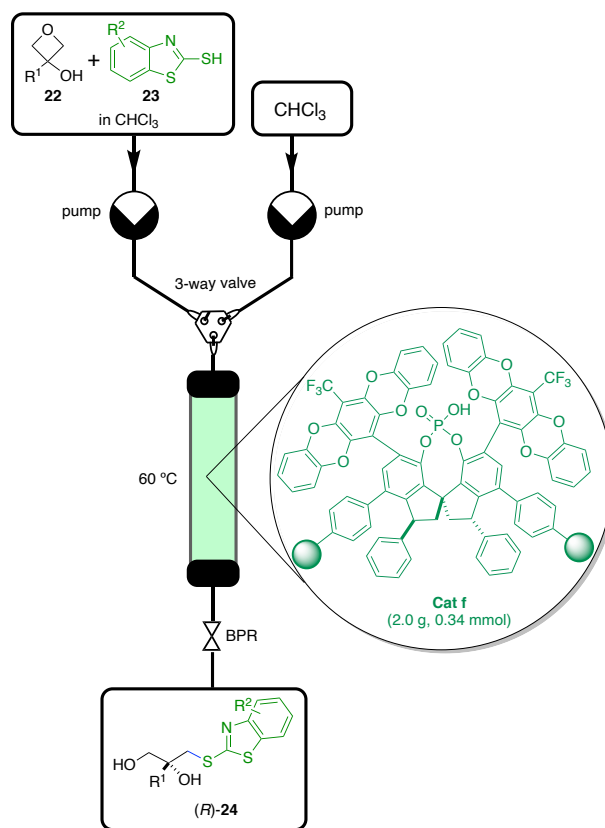


Figure 4. Schematic representation of the flow system for the desymmetrization of oxetanes mediated by the PS-supported SPA **Cat f**.

The same flow system, with the same catalyst sample, was next used for the study of the scope of the desymmetrization process by reaction of **22a-n** with **23a-d**. For this study, we selected 3,3-disubstituted oxetanes as substrates. Besides having been comparatively less studied, they offer the additional interest of leading to products with a quaternary stereocenter. All the experiments were sequentially performed with 2 mmol of **22** and 2.5 mmol of **23** in 20 mL CHCl₃, operating the flow system at 0.5 mL/min. In this manner, every individual experiment lasted 40 minutes, and the packed bed reactor was rinsed for 20 min with CHCl₃ between individual experiments in order to remove traces of the previous product (Figure 5). In this manner, a family of fourteen different oxetanes **22a-n** was submitted to the desymmetrization process in flow in combination with the mercaptobenzothiazoles **23a-d** to produce the seventeen products depicted in Figure 5. The process tolerates well a variety of substituent types at C3 on the oxetane structure (aryl, heteroaryl, alkyl, alkenyl, alkynyl) defining in most cases tertiary alcohols at that position. In the same manner, substituents on the aromatic ring of **23** do not affect in a substantial manner the outcome of the reaction with the same oxetane (**22a**).

From the point of view of yield, it is important to remark that all the studied desymmetrization reactions are very clean, no significant byproducts being detected. Thus, although lower than optimal yields detected in some cases (>65%), it should be possible to increase them by simply adjusting flow rate in those particular examples. As for enantioselectivity, the results in Figure 5 tend to indicate that the differences between the steric requirements of the C3 substituents on the oxetane ring play a fundamental role on the outcome of the reaction. In tertiary alcohol-type substrates, the presence of an aromatic substituent at C3 generally leads to very high *ee*, whereas in the parallel cases involving linear alkyl substituents, a certain chain length is required for high enantioselectivity (37% *ee* in **24ha**, where R¹ = methyl, but 90% *ee* in **24ia**, where R¹ = butyl).

The success of the desymmetrization in the case of product **24ea**, containing a terminal propargyl alcohol moiety, offers an additional interest. Thus, this type of substrates easily undergo copper-catalyzed alkyne-azide (CuAAC) reactions in continuous flow,⁷³ and the integration of these two constructive reactions can lead to the telescoped, highly convergent preparation of modular enantioenriched triazoles.

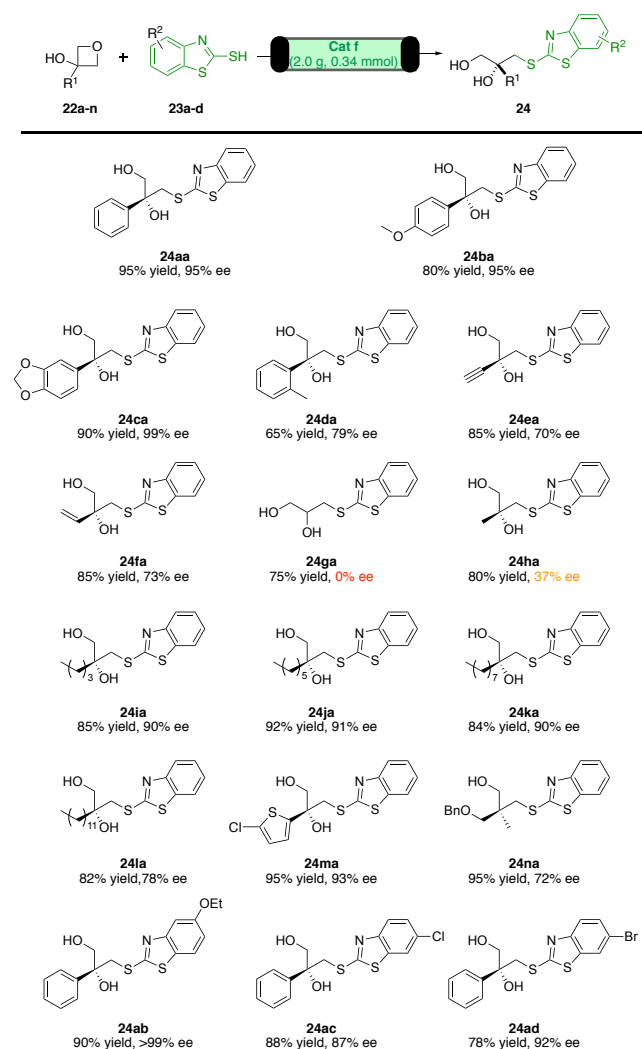
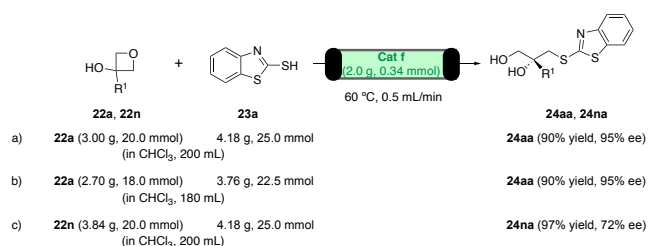


Figure 5. Oxetanes and benzothiazolethiols scope in the **Cat f** catalyzed desymmetrization reaction. All yields shown refer to isolated products. The reactions were performed with oxetane **22** (2 mmol) and benzothiazolethiol **23** (2.5 mmol) in 20 mL chloroform, flowing for 40 minutes (flow rate = 0.5 ml/min) through a packed bed reactor at 60 °C containing 2.0 g (0.34 mmol) of **Cat f**. When the circulation of a given reactants mixture was complete,

chloroform was circulated through the reactor for 20 minutes at 0.5 mL/min. Then the system is ready for the next reactant combination.

As a final test of the practical value of the desymmetrization in continuous flow catalyzed by **Cat f**, we planned to use the same packed bed reactor employed for the scope in Figure 5 for the gram scale preparation of **24aa** (two runs) and **24na**. In a first preparative experiment (Scheme 3, a), starting from 20 mmol of **22a** and 25 mmol of **23a** in chloroform (200 mL) the system was operated at 0.5 mL/min for *ca.* 400 minutes, till the reactants solution had completely circulated, and the packed bed reactor was then washed by circulating chloroform at 0.5 mL/min for 20 minutes. Product purification by the usual protocol afforded **24aa** (5.7g, 90% yield) with 95% *ee*. In the same manner, **22a** (0.24 g, 92% conversion) was recovered. After keeping the employed sample of **Cat f** for 15 months, the flow preparation of **24aa** was performed again under identical conditions, starting from 18 mmol of **22a** and 22.5 mmol of **23a** in chloroform (180 mL) (Scheme 3, b). Gratifyingly, both yield and enantioselectivity of the previous run were reproduced. Subsequently, the preparation of **24na** was also performed at the 20 mmol scale using one more time the same packed bed reactor (Scheme 3, c), a slight improvement in yield and the same enantioselectivity with respect to the smaller scale preparation in Figure 5 being recorded. Thus, all the data collected in our study, from recycling in batch to sequential scoping in flow and use at the multigram scale in flow point out to the important robustness of **Cat f** and its suitability for large scale production. In this respect it is worth mentioning that, setting apart the initial adjustment of flow parameters (Table S3), the 0.34 mmol sample of **Cat f** used for the scope in Figure 5 and the preparative experiments in Scheme 3 accounts for a cumulative TON of *ca.* 243, without decreases in performance.

Scheme 3. Continuous flow preparation of **24aa** in gram scale using a multiply reused sample of **Cat f**.



In order to rationalize the enantioselectivity performance of **Cat f** and the differences with the poorly behaving **Cat b**, we decided to undertake a theoretical study of the desymmetrization process. Early computational studies on organocatalytic reactions mediated by chiral phosphoric acids include Mannich reaction, 1,3-dipolar cycloadditions^{74a} as well as desymmetrization processes.^{74b-c} In particular, Seguin and Wheeler studied the desymmetrization of 3-substituted oxetanes catalyzed by 6,6'-bis(9-anthryl)SPINOL phosphoric acid, reaching the conclusion that competing noncovalent interactions are the main factor controlling enantioselectivity in that case.⁷⁵ The main focus of the present computational study has been directed to establishing the relevance of the pentacyclic substituents at the 6,6'-positions of **Cat f** in biasing the enantioselectivity of the oxetane desymmetrizations mediated by this species. **Cat b** and **Cat f** were selected for the computational study as they represent the two extremes in the size of the substituents at the 6,6'-positions and of recorded enantioselectivity. Since the experimental studies

described in this manuscript indicate that the polymer backbone does not severely affect enantioselectivity with respect to homogeneous models (see Table 2 below), the truncated models **25** and **26** of the real catalysts were used in the calculations (Figure 6).

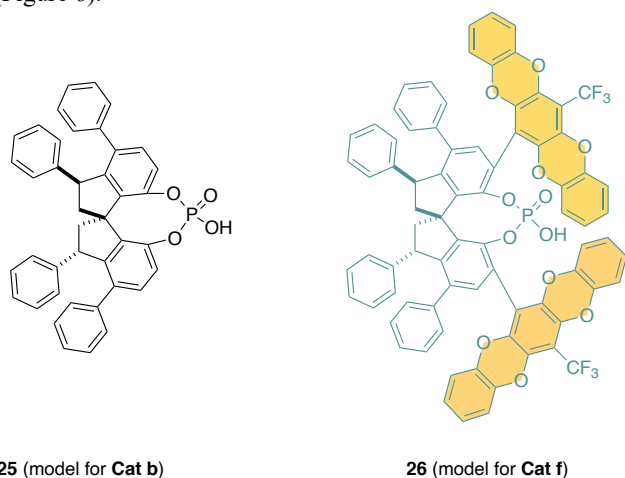


Figure 6. Structures **25** and **26**, models for **Cat b** and **Cat f**, respectively, in the theoretical studies.

Focusing first our attention onto the reactants, we were surprised to find that the thiol tautomeric form of the reactant benzo[d]thiazole-2-thiol is not involved in the catalytic nucleophilic attack onto the 3-hydroxyoxetane structure. At the employed level of theory (M06-2X-D3/DGTZVP/SMD//M06-2X-D3/DGDZVP) the results of the theoretical studies suggest that the tautomeric form of **23a**, benzo[d]thiazole-2(3H)-thione, keto-**23a**, is thermodynamically preferred over the thiol form by $\Delta G = -8.4 \text{ kcal}\cdot\text{mol}^{-1}$ at 333 K (Figure 7). The interconversion between enethiol and thione tautomers can take place in either intermolecular or intramolecular fashions. In the former case, the calculated barrier is very low, $\Delta G^\ddagger = +6.0 \text{ kcal}\cdot\text{mol}^{-1}$, while the intramolecular process is not competitive at the considered temperature ($\Delta G^\ddagger = +29.8 \text{ kcal}\cdot\text{mol}^{-1}$). It is thus suggested that only the thione form of **23a** will be present in the reaction media and will likewise be the nucleophile acting in the desymmetrization reaction.

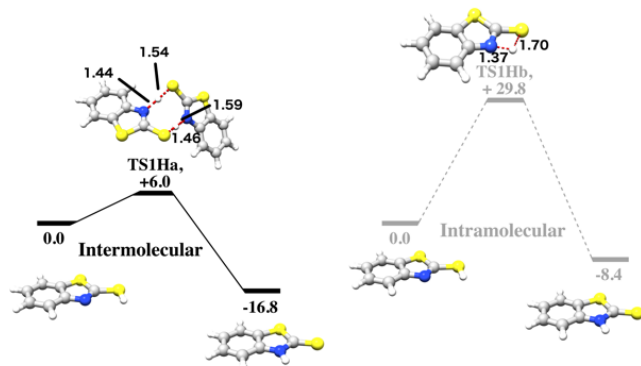


Figure 7. Free energy profiles for the intermolecular and the intramolecular tautomerization of benzo[d]thiazole-2-thiol (**23a**) into benzo[d]thiazole-2-thione (keto-**23a**) in CHCl_3 at 333K. Displacements associated to the imaginary frequencies in the relevant transition states are indicated by red dotted lines and related atomic distances in Å.

Xie and coworkers were able to isolate tautomeric 2-(methylthio)benzo[d]thiazole (**27a**) and 3-methylbenzo[d]thiazole-2(3H)-thione (**27b**) prepared through different synthetic routes

and characterize them by NMR spectroscopy.⁷⁶ As expected, the thiol and thione tautomers present very different chemical shift in $^{13}\text{C}\{^1\text{H}\}$ NMR: $\delta = 167.0 \text{ ppm}$ for C-SH , and $\delta = 188.4 \text{ ppm}$ for C=S .⁷⁶ To determine the tautomeric form of **23** present in solution, we measured the $^{13}\text{C}\{^1\text{H}\}$ NMR spectrum on a freshly prepared sample of the reagent. A chemical shift of 190.9 ppm was found for the considered carbon, strongly suggesting that **27b** is the largely predominant tautomer present in CHCl_3 solution at 298 K (Figure 8). Moreover, a full geometrical optimization of a Van der Waals complex featuring the contact of a molecule of **23a** with **25** triggers a barrierless proton exchange to form keto-**23a**.

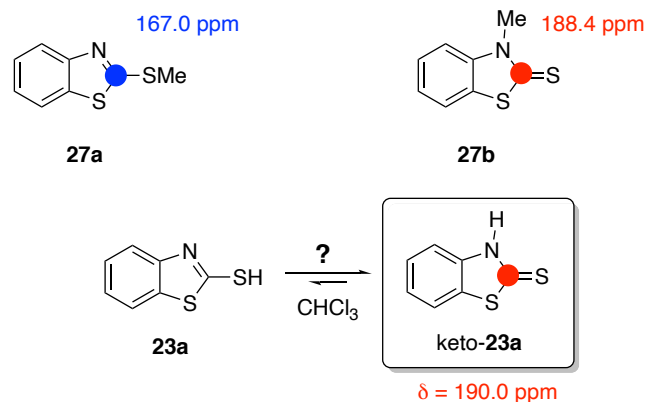


Figure 8. Tautomeric equilibrium of **23a** in chloroform

Interestingly, the benzo[d]thiazole-2(3H)-thione tautomer (keto-**23a**) exhibits nucleophilic character and easily undergoes nucleophilic attack to the oxetane partner in the presence of phosphoric acid catalysts. Figure 9 shows the calculated reaction profile for the reaction of **22a** with keto-**23a** catalyzed by the **Cat b** truncated model, **25**. Mechanistic information from the intrinsic reaction coordinates (IRC) following the hypersurface downhill from the transition states suggests that proton transfer from the catalyst to the ether oxygen of the oxetane ring happens first, followed by a nucleophilic attack of the thione sulphur atom onto one of the enantiotopic carbon atoms α to oxygen in the oxetane ring (C2 or C4). The transition states for these desymmetrizing processes exhibit marked $\text{S}_{\text{N}}2$ characteristics, with $\text{O}\cdots\text{C}\cdots\text{S}$ angle of nearly 180° . As already pointed out by Seguin and Wheeler,⁷⁴ the shape of the oxetanol substrate provides a perfect interlocking match with the phosphoric acid catalyst via the formation of two complementary $\text{O-H}\cdots\text{O}$ hydrogen interactions. The result is the formation of a stable Van der Waals adduct between oxetanol **22a** and **25** (**10_1** in Figure 9). We also investigated the possible involvement of a similar Van der Waals complex of **25** with keto-**23a** in the early stages of the reaction; however, its higher endergonic nature (compared to **10_1**) discarded it as a competent reaction intermediate.

To get a more comprehensive scenario of the possible transition states involved in the desymmetrization process, we considered four different geometric catalyst-to-reactants approaches, including two (*R*)- and two (*S*)-stereodifferentiating pathways. In this respect, Figures 9 and 10 show the lowest energetically demanding pathways leading to (*R*)- and (*S*)-stereoisomers in processes mediated by **25** and **26**, respectively (data concerning redundant transition structures and minima thereof are included in the computational section of Supporting Information). Calculations at the M06-2X-D3/DGTZVP/SMD//M06-2X-D3/DGDZVP level estimate the reaction barrier for the process mediated by **25** as $+25.5 \text{ kcal}\cdot\text{mol}^{-1}$ for the (*R*)-directing **TS1d_R** and $+26.3 \text{ kcal}\cdot\text{mol}^{-1}$

for (*S*)-directing **TSb_S**, Figure 9. This results in a calculated enantioselectivity at 333 K of 78:22 (65:35 without BSSE corrections) in favor of the *R* enantiomer ($ee_R = 55\%$ with BSSE corrections and $ee_R = 29\%$ without BSSE corrections). These data are in excellent agreement with the experimental results obtained with **Cat b** at the same temperature ($ee_R = 20\%$).

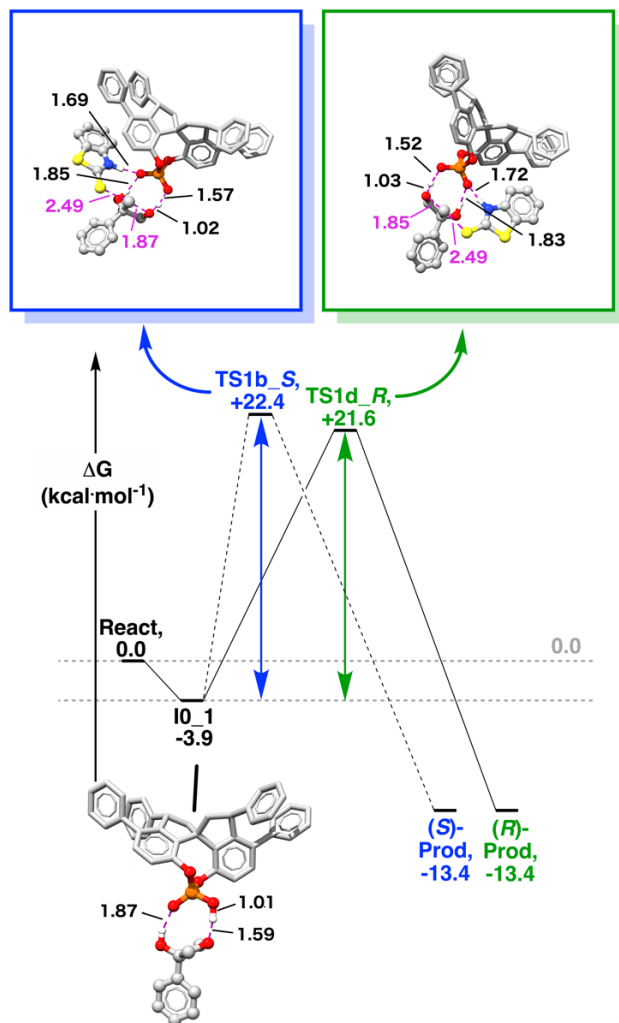


Figure 9. Free energy profiles for the desymmetrization of **22a** with keto-**23a** catalyzed by the **Cat b** model (**25**). The values are reported in kcal·mol⁻¹. **IO_1** represents the resting states of the catalyst. Relevant hydrogen bonds distances are reported in black (in Å). Relevant distances associated to displacements of the imaginary frequency for transition states are reported in magenta (in Å).

Figure 10 shows the calculated reaction profile for the reaction of **22a** with keto-**23a** catalyzed by the **Cat f** truncated model, **26**. The first substantial difference between catalysts **25** and **26** is that the latter binds the substrates in a somewhat stronger manner than the former, as it can be seen in the coordination of the oxetanol at **IO_1** in Figure 10. Thus, **26** binds the oxetanol exergonically with a net gain of up to -13.2 kcal·mol⁻¹, while **25** binds oxetanol with a net gain up to -3.9 kcal·mol⁻¹ (as comparison, an intermediate situation is seen for **Cat a**, with a net gain of up to -6.5 kcal·mol⁻¹, see Supporting information). Consequently, while **25** expels easily the products at the end of the desymmetrization (the value of -13.4 kcal·mol⁻¹ in Figures 9 and 10 refers to the separation of the product and catalyst at infinite distance), the product of the desymmetrization prefers

to remain bound to catalyst **26** than to be separated from it. Catalyst-product adduct resides at -26.3 kcal·mol⁻¹ in the free energy profile of Figure 10. In the case of **26** the system must pay an energetic penalty of +12.9 kcal·mol⁻¹ to free the catalytic site and allows the release of the (*R*)-product (again, an intermediate situation is seen for **Cat a**, whose catalyst-product adduct resides at -18.6 kcal·mol⁻¹ and the system has to pay a penalty of +5.2 kcal·mol⁻¹ to free the catalytic site, see Supporting Information).

Secondly, **26** displays an enhanced reactivity towards the desymmetrization of **22a** with **23a**: the lowest free energy barrier stands out at +20.3 kcal·mol⁻¹, five kcal·mol⁻¹ lower than that shown for catalysis carried out by **25**. Thus, the results of these calculations suggest that **Cat f** will kinetically outperform even **Cat a**, whose activation barrier stands out at +21.5 kcal·mol⁻¹ (see Supporting Information) and correctly reproduces the experimental enantioselectivity recorded for **Cat f** at 333 K, of up to $ee \sim 98\%$ (calculated ee is 100% with and without BSSE correction). The predominance of *R* product arises from **TS1d_R**, represented in Figure 10 in side and bottom views. For comparison, calculations at the same level of theory also correctly predicts $ee \sim 100\%$ for **Cat a** (see Supporting Information).

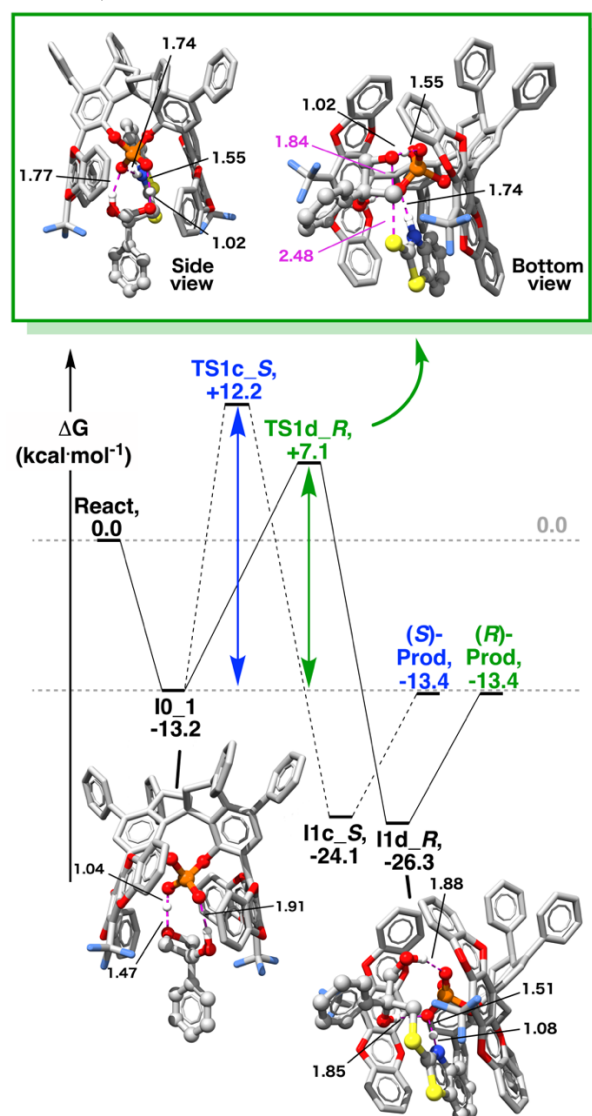


Figure 10. Free energy profiles for the desymmetrization of **22a** with keto-**23a** catalyzed by the **Cat f** model (**26**). The values are

reported in kcal·mol⁻¹. **10_1** represents the resting states of the catalyst. Relevant hydrogen bond distances are represented in black (in Å). Relevant distances associated to displacements following the imaginary frequency for transition states are represented in magenta (in Å).

The stronger binding towards the substrates seen for **26**, compared to **25**, can be rationalized considering that the extended heteroaromatic wings do not only create a deep chiral groove of steric nature around the catalytic center but, even more importantly, they also offer extra differential stabilization via non-covalent interactions and π - π stacking. Figure 11a represents δg^{inter} isosurfaces mapping the non-covalent interactions between the anionic catalyst (Fragment 1, [(RO)₂PO₂]⁻) and the protonated activated complex of the substrates (Fragment 2, Oxetanol + keto-**23a** + H⁺) via Independent Gradient Model (IGM), developed by Henon and coworkers⁷⁷ and implemented by Lu and coworkers in MULTIWFN.⁷⁸ We found over 1300 weak interactions in **TS1d_R** of **26** including strong interfragment O-H...O and N-H...O hydrogen bonds, a plethora of F...C, F...O, F...H, S...O, S...F and S...C Van der Waals contacts and other interactions assimilable to π - π stacking. The cumulative effect of these weak interactions within **26** is so strong that the extended heteroaromatic conjugation of the wings is overcome, enabling the loss of planarity and the formation of a “templated” cradle around the catalytic center, reminiscent to the *induced fit* operating in enzymes.⁷⁹

Figure 11b displays a quantitative measurement of these weak interactions at transition states between anionic catalyst (Fragment 1) and the protonated activated complex of the substrates (Fragment 2) for **Cat a**, **Cat b** (**25**) and **Cat f** (**26**): $\Delta PE_{\text{TS}(R)}$ and $\Delta PE_{\text{TS}(S)}$ represent the molar work (i.e., a difference of potential energies) that must be spent in order to separate Frag. 1 and 2 at infinite distance in chloroform, with a dielectric constant $\epsilon = 4.7113$, for (*R*)-directing TS and (*S*)-directing TS, respectively. Figure 11b conveys two fundamental concepts at glance: firstly, the **Cat f** model binds the (*R*)-activated complex 3.4 kcal·mol⁻¹ stronger than **Cat a** and 19.6 kcal·mol⁻¹ stronger than **Cat b** model (**25**) at transition state in chloroform and, secondly, the fragments within (*R*)-stereoinducing transition state are tighter bound than those in (*S*)-stereoinducing transition state for **Cat f** (and **Cat a**) compared to **Cat b** (the difference between $\Delta PE_{\text{TS}(R)}$ and $\Delta PE_{\text{TS}(S)}$ is essentially negligible for **25**, even more so considering that it is of the same order of magnitude as the differences between the (*R*)- and (*S*)-directing isolated fragments, $\Delta PE_{\text{Frag}\#1}$ and $\Delta PE_{\text{Frag}\#2}$, Figure 11). This is an unequivocal sign that cumulative weak interactions between Frag. 1 and 2 at (*R*)-stereoinducing **TS1d_R** of **Cat f** are competitively stronger than those within the fragments in (*S*)-stereoinducing **TS1c_S**, causing an overall increased stabilization of the former structure over the latter.

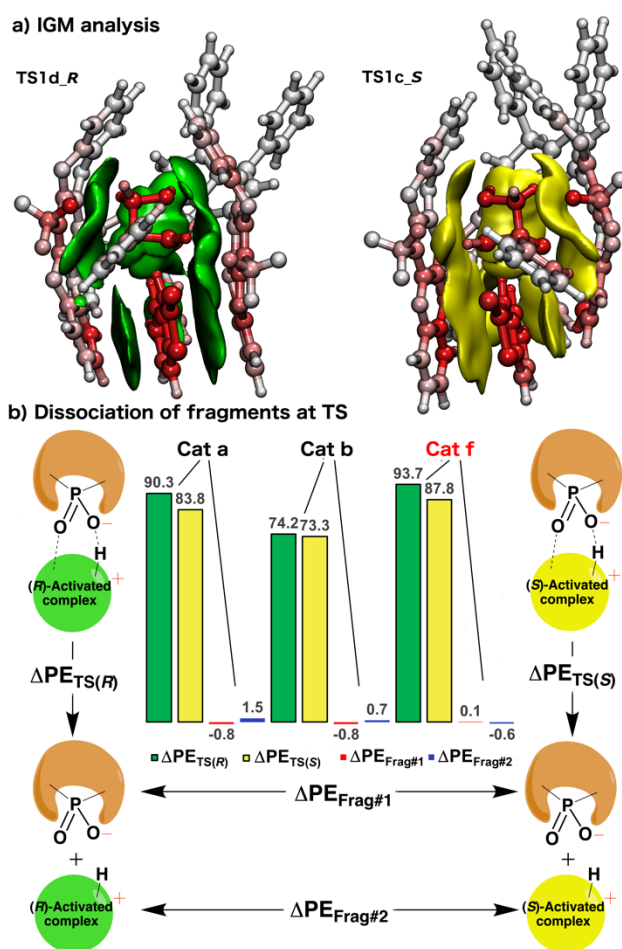


Figure 11. a) IGM on computational densities for **TS1d_R** and **TS1c_S** structures in reactions mediated by **Cat f** model (**26**). Green and yellow Δg^{inter} surfaces represent non-covalent interaction regions between anionic catalyst (Frag#1) and protonated activated complex of substrates (Frag#2) at 0.004 a.u. isovalue. The darker the red color of the atoms, the more they contribute to the Δg^{inter} isosurface (atoms in grey do not contribute). b) Energetics of the dissociation of Fragment 1 and Fragment 2 at transition states. Values are in kcal·mol⁻¹, being only valid for reactions in chloroform.

At the light of the results of the theoretical study, where the role of the pentacyclic substituents at 6,6' on the enantioselectivity recorded with **Cat f** in the catalytic desymmetrization of 3,3-disubstituted oxetanes has been stressed, we considered the potential interest of developing a minimalistic, readily available analog of this species for work in homogeneous phase. Since substitution at 4,4' is required for immobilization, but does not seem to play an important role on enantioselectivity according to the calculated structures for the relevant transition states (see Figures 10 and 11), we conceived **Cat g** as the candidate structure fulfilling the above conditions.

As shown in Scheme 4, **Cat g** could be prepared in only two steps from intermediate **14** in 45% yield (or in four steps, with 38% overall yield, from **12**) using transformations already optimized in the preparation of other catalysts in this study. With **Cat g** in hands, its use in the catalytic desymmetrization of a representative family of oxetanes **22** was studied. We have collected in Table 2 the results of this study. For comparison purposes, the results obtained with **Cat f** in continuous flow have also been included.

Scheme 4. Preparation of the monomeric phosphoric acid **Cat g** from intermediate **14**.

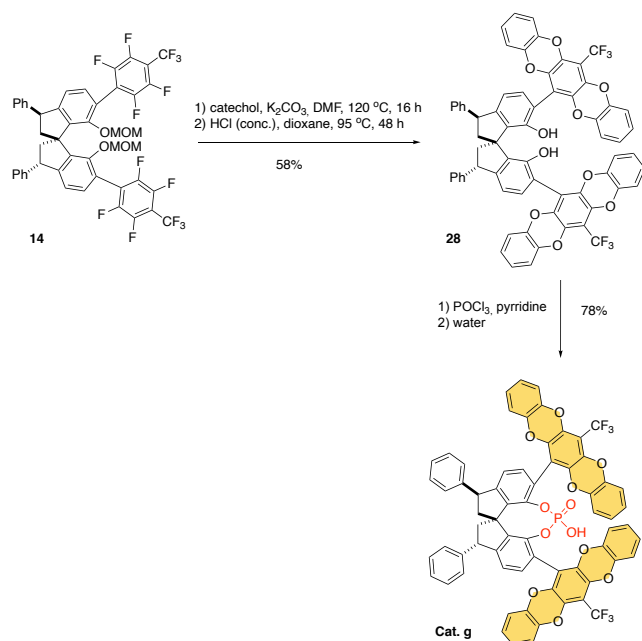


Table 2. Desymmetrization of **22** with **23** leading to **24** mediated by the homogeneous catalyst **Cat g**.^a

Entry	Product	with Cat g	
		Yield [%]; ee [%]	Yield [%]; ee [%] ^b
1	24aa	87; 95	95; 95
2	24ba	78; 98	80; 95
3	24ca	83; >99	90; 99
4	24da	86; 95	65; 79
5	24ea	90; 73	85; 70
6	24ga	84; 7 ^c	75; 0
7	24ha	87; 13 ^d	80; 37
8	24ia	90; 90	85; 90
9	24ja	85; 92	92; 91
10	24ka	88; 92	84; 90
11	24ma	87; 97	95; 93
12	24na	95; 78	95; 72
13	24ab	96; 95	90; >99
14	24ac	85; 85	88; 87
15	24ad	80; 74	78; 92

^aStandard conditions: **22** (0.2 mmol), **23** (0.25 mmol) and **Cat g** (12 mg, 5 mol%) in chloroform (4 mL) stirred at 60 °C (oil bath temp) in a sealed vial for 16 h. ^bReaction conditions are those in Figure 5.

^cWhen the reaction was performed at rt for 16 h, yield was 82% and ee 4%. ^dWhen the reaction was performed at rt. for 16 h, yield was 86% and ee 10%.

To facilitate comparison with **Cat f**, the scope of the desymmetrization with **Cat g** was studied in chloroform solution at 60 °C. Under these conditions, the parallelism with **Cat f** in terms

of performance is remarkable. Thus, the preparations of **24ga** and **24ha** turned out to be poorly enantioselective, as it is the case with **Cat f**. For the rest of products **24**, although some differences can be noted in individual cases, the average yield and enantioselectivity recorded with the heterogeneous (**Cat f**) and the simplified homogeneous catalyst (**Cat g**) are essentially identical: 86.9% average yield with **Cat g** vs. 86.3% with **Cat f**, and 89.5% average ee with **Cat g** vs. 88.6% with **Cat f**. All together, these results tend to indicate that the pentacyclic substituents present at the 6,6' positions of **Cat f**, possess the power to impart optimal enantiocontrol characteristics to SPINOL-derived phosphoric acids without the need of other structural characteristics.

In summary, a family of chiral phosphoric acids derived from 3,3'-diphenyl-SPINOL (SPAs) been successfully synthesized and immobilized onto cross-linked polystyrene using either the 4,4' or the 6,6' positions. The resulting catalytic polymers efficiently mediate the desymmetrization of 3-substituted oxetanes (**22**) with 3-mercaptobenzothiazoles (**23**). The optimal catalyst (**Cat f**) involves immobilization through positions 4,4', remote from the catalytic site, and presents two very extended heteroaromatic substituents at positions 6,6'. **Cat f** exhibits unlimited recyclability (to the extent of the attempted reuses) in batch and flow, providing the target desymmetrized products in high yield (up to 92%) and enantioselectivity and (up to >99% ee), high productivity being recorded under both types of experimental conditions. A DFT study on monomer models of **Cat b** and **Cat f**, the worst and the best-performing SPAs in this study, has demonstrated that the extended, geometrically adaptable heteroaromatic wings at the 6,6' positions of the SPINOL skeleton in **Cat f** are key to improved kinetics and enantioselectivity in the desymmetrization process thanks to extended and cumulatively strong non-covalent interactions. The lessons learned from this theoretical study have guided the design of a readily available, minimalistic homogeneous analog (**Cat g**) with catalytic performance similar to **Cat f**, that could represent an interesting and economic alternative when single catalytic use in batch is considered.

Notes

The authors declare no competing financial interest.

AUTHOR INFORMATION

Corresponding Author

Miquel A. Pericàs – Institute of Chemical Research of Catalonia (ICIQ), The Barcelona Institute of Science and Technology (BIST), Av. Països Catalans, 16, 43007 Tarragona (Spain); Departament de Química Inorgànica i Orgànica, Universitat de Barcelona, 08028 Barcelona, Spain; orcid.org/0000-0003-0195-8846; Email: mapericas@iciq.es

Authors

Junshan Lai – Institute of Chemical Research of Catalonia (ICIQ), The Barcelona Institute of Science and Technology (BIST), Av. Països Catalans, 16, 43007 Tarragona (Spain); Universitat Rovira i Virgili, Departament de Química Analítica i Química Orgànica, c/Marcel·lí Domingo, 1, 43007 Tarragona (Spain)
Mauro Fianchini – Institute of Chemical Research of Catalonia (ICIQ), The Barcelona Institute of Science and Technology (BIST), Av. Països Catalans, 16, 43007 Tarragona (Spain); orcid.org/0000-0003-2619-7932. Inquiries on computational aspects of the manuscript should be addressed to this author at: mfianchini@iciq.es

ASSOCIATED CONTENT

Supporting Information. The Supporting Information is available free of charge on the ACS Publications website at <http://pubs.acs.org>.

Synthetic procedures and complete spectroscopic (NMR and HPLC) characterizations of the catalytic structures and their precursors. Synthetic procedures of immobilization of catalysts onto polystyrene stationary phase, full methodology of the flow chemistry implementation, complete characterization of all the products (NMR and HPLC). Cartesian coordinates and frequencies of all characterized stationary points, absolute values of thermodynamic state functions, absolute and relative values of RRHO-corrected thermodynamic state functions (PDF)

Accession Codes. CCDC 2018564 contains the supplementary crystallographic data for this paper. These data can be obtained free of charge via www.ccdc.cam.ac.uk/data_request/cif, or by emailing data_request@ccdc.cam.ac.uk, or by contacting The Cambridge Crystallographic Data Centre, 12 Union Road, Cambridge CB2 1EZ, UK; fax: +44 1223 336033.

ACKNOWLEDGMENT

This work was funded by MINECO/FEDER (grants CTQ2015-69136-R and PID2019-109236RB-I00) and the CERCA Program/Generalitat de Catalunya. We also thank Ministerio de Ciencia, Innovación y Universidades (Spain) for support through Severo Ochoa Excellence Accreditation 2020-2023 (CEX2019-000925-S, MIC/AEI). J. L. thanks the MINECO for a FPI fellowship (BES-2016-078937). MF would like to thank Prof. E. Henon and Prof. T. Lu for the useful discussions on the nature and the implementation of Independent Gradient Model (IGM).

REFERENCES

- Kampen, D.; Reisinger, C. M.; List, B. Chiral Brønsted Acids for Asymmetric Organocatalysis. In *Asymmetric Organocatalysis*, List, B., Ed. Springer Berlin Heidelberg: Berlin, Heidelberg, 2009; pp 1-37.
- Akiyama, T.; Itoh, J.; Fuchibe, K. Recent Progress in Chiral Brønsted Acid Catalysis. *Adv. Synth. Catal.* **2006**, *348* (9), 999-1010.
- Akiyama, T. Stronger Brønsted Acids. *Chem. Rev.* **2007**, *107* (12), 5744-5758.
- Connon, S. J. Chiral Phosphoric Acids: Powerful Organocatalysts for Asymmetric Addition Reactions to Imines. *Angew. Chem. Int. Ed.* **2006**, *45*, 3909-3912.
- Ouellet, S. G.; Walji, A. M.; Macmillan, D. W. C. Enantioselective Organocatalytic Transfer Hydrogenation Reactions using Hantzsch Esters. *Acc. Chem. Res.* **2007**, *40*, 1327-1339.
- Akiyama, T.; Itoh, J.; Yokota, K.; Fuchibe, K., Enantioselective Mannich-Type Reaction Catalyzed by a Chiral Brønsted Acid. *Angew. Chem. Int. Ed.* **2004**, *43*, 1566-1568.
- Uraguchi, D.; Terada, M. Chiral Brønsted Acid-Catalyzed Direct Mannich Reactions via Electrophilic Activation. *J. Am. Chem. Soc.* **2004**, *126*, 5356-5357.
- Taylor, M. S.; Jacobsen, E. N., Asymmetric Catalysis by Chiral Hydrogen-Bond Donors. *Angew. Chem. Int. Ed.* **2006**, *45*, 1520-1543.
- Doyle, A. G.; Jacobsen, E. N. Small-Molecule H-Bond Donors in Asymmetric Catalysis. *Chem. Rev.* **2007**, *107*, 5713-5743.
- Dondoni, A.; Massi, A., Asymmetric Organocatalysis: From Infancy to Adolescence. *Angew. Chem. Int. Ed.* **2008**, *47*, 4638-4660.
- Terada, M. Binaphthol-Derived Phosphoric Acid as a Versatile Catalyst for Enantioselective Carbon-Carbon Bond Forming Reactions. *Chem. Commun.* **2008**, 4097-4112.
- Adair, G.; Mukherjee, S.; List, B. TRIP-A Powerful Brønsted Acid Catalyst for Asymmetric Synthesis. *Aldrichimica Acta* **2008**, *41*, 31-39.
- You, S.-L.; Cai, Q.; Zeng, M. Chiral Brønsted Acid Catalyzed Friedel-Crafts Alkylation Reactions. *Chem. Soc. Rev.* **2009**, *38*, 2190-2201.
- Terada, M. Chiral Phosphoric Acids as Versatile Catalysts for Enantioselective Transformations. *Synthesis* **2010**, 1929-1982.
- Yu, J.; Shi, F.; Gong, L.-Z. Brønsted-Acid-Catalyzed Asymmetric Multicomponent Reactions for the Facile Synthesis of Highly Enantioenriched Structurally Diverse Nitrogenous Heterocycles. *Acc. Chem. Res.* **2011**, *44*, 1156-1171.
- Rueping, M.; Kuenkel, A.; Atodiresei, I. Chiral Brønsted Acids in Enantioselective Carbonyl Activations—Activation Modes and Applications. *Chem. Soc. Rev.* **2011**, *40*, 4539-4549.
- Parmar, D.; Sugiono, E.; Raja, S.; Rueping, M. Complete Field Guide to Asymmetric BINOL-Phosphate Derived Brønsted Acid and Metal Catalysis: History and Classification by Mode of Activation; Brønsted Acidity, Hydrogen Bonding, Ion Pairing, and Metal Phosphates. *Chem. Rev.* **2014**, *114*, 9047-9153.
- Wu, H.; He, Y.-P.; Shi, F. Recent Advances in Chiral Phosphoric Acid Catalyzed Asymmetric Reactions for the Synthesis of Enantiopure Indole Derivatives. *Synthesis* **2015**, *47*, 1990-2016.
- Merad, J.; Lalli, C.; Bernadat, G.; Maury, J.; Masson, G., Enantioselective Brønsted Acid Catalysis as a Tool for the Synthesis of Natural Products and Pharmaceuticals. *Chem. Eur. J.* **2018**, *24*, 3925-3943.
- Maji, R.; Mallojija, S. C.; Wheeler, S. E. Chiral Phosphoric Acid Catalysis: from Numbers to Insights. *Chem. Soc. Rev.* **2018**, *47*, 1142-1158.
- Xing, C.-H.; Liao, Y.-X.; Ng, J.; Hu, Q.-S. Optically Active 1,1'-Spirobiindane-7,7'-diol (SPINOL)-Based Phosphoric Acids as Highly Enantioselective Catalysts for Asymmetric Organocatalysis. *J. Org. Chem.* **2011**, *76*, 4125-4131.
- Birman, V. B.; L. Rheingold, A.; Lam, K.-C., 1,1'-Spirobiindane-7,7'-diol: a Novel, C₂-Symmetric Chiral Ligand. *Tetrahedron: Asymmetry* **1999**, *10*, 125-131.
- Xie, J.-H.; Zhou, Q.-L. Chiral Diphosphine and Monodentate Phosphorus Ligands on a Spiro Scaffold for Transition-Metal-Catalyzed Asymmetric Reactions. *Acc. Chem. Res.* **2008**, *41*, 581-593.
- Chung, Y. K.; Fu, G. C. Phosphine-Catalyzed Enantioselective Synthesis of Oxygen Heterocycles. *Angew. Chem. Int. Ed.* **2009**, *48*, 2225-2227.
- Čorić, I.; Müller, S.; List, B. Kinetic Resolution of Homoaldols via Catalytic Asymmetric Transacetalization. *J. Amer. Chem. Soc.* **2010**, *132*, 17370-17373.
- Xu, F.; Huang, D.; Han, C.; Shen, W.; Lin, X.; Wang, Y. SPINOL-Derived Phosphoric Acids: Synthesis and Application in Enantioselective Friedel-Crafts Reaction of Indoles with Imines. *J. Org. Chem.* **2010**, *75*, 8677-8680.
- Rahman, A.; Lin, X. Development and Application of Chiral Spirocyclic Phosphoric Acids in Asymmetric Catalysis. *Org. Biomol. Chem.* **2018**, *16*, 4753-4777.
- Li, J.; Chen, G.; Wang, Z.; Zhang, R.; Zhang, X.; Ding, K. Spiro-2,2'-bichroman-Based Bisoxazoline (SPANbox) Ligands for Zn^{II}-Catalyzed Enantioselective Hydroxylation of β -Keto Esters and 1,3-Diester. *Chem. Sci.* **2011**, *2*, 1141-1144.
- Wang, X.; Han, Z.; Wang, Z.; Ding, K. Catalytic Asymmetric Synthesis of Aromatic Spiroketal by SpinPhox/Iridium(I)-Catalyzed Hydrogenation and Spiroketalization of α,α' -Bis(2-hydroxyarylidene) Ketones. *Angew. Chem. Int. Ed.* **2012**, *51*, 936-940.
- Li, S.; Zhang, J.-W.; Li, X.-L.; Cheng, D.-J.; Tan, B. Phosphoric Acid-Catalyzed Asymmetric Synthesis of SPINOL Derivatives. *J. Am. Chem. Soc.* **2016**, *138*, 16561-16566.
- Sun, W.; Gu, H.; Lin, X. Synthesis and Application of Hexamethyl-1,1'-spirobiindane-Based Phosphine-Oxazoline Ligands in Ni-Catalyzed Asymmetric Arylation of Cyclic Aldimines. *J. Org. Chem.* **2018**, *83*, 4034-4043.
- Huang, J.; Hong, M.; Wang, C.-C.; Kramer, S.; Lin, G.-Q.; Sun, X.-W. Asymmetric Synthesis of Chiral Spiroketal Bisphosphine Ligands and Their Application in Enantioselective Olefin Hydrogenation. *J. Org. Chem.* **2018**, *83*, 12838-12846.
- Chen, G.-Q.; Lin, B.-J.; Huang, J.-M.; Zhao, L.-Y.; Chen, Q.-S.; Jia, S.-P.; Yin, Q.; Zhang, X. Design and Synthesis of Chiral oxa-Spirocyclic Ligands for Ir-Catalyzed Direct Asymmetric Reduction of Bringmann's Lactones with Molecular H₂. *J. Am. Chem. Soc.* **2018**, *140*, 8064-8068.
- Argüelles, A. J.; Sun, S.; Budaitis, B. G.; Nagorny, P. Design, Synthesis, and Application of Chiral C₂-Symmetric Spiroketal-Containing Ligands in Transition-Metal Catalysis. *Angew. Chem. Int. Ed.* **2018**, *57*, 5325-5329.

35. Zheng, Z.; Cao, Y.; Chong, Q.; Han, Z.; Ding, J.; Luo, C.; Wang, Z.; Zhu, D.; Zhou, Q.-L.; Ding, K. Chiral Cyclohexyl-Fused Spiroindanes: Practical Synthesis, Ligand Development, and Asymmetric Catalysis. *J. Am. Chem. Soc.* **2018**, *140*, 10374-10381.
36. Yin, L.; Xing, J.; Wang, Y.; Shen, Y.; Lu, T.; Hayashi, T.; Dou, X. Enantioselective Synthesis of 3,3'-Diaryl-SPINOLs: Rhodium-Catalyzed Asymmetric Arylation/BF₃-Promoted Spirocyclization Sequence. *Angew. Chem. Int. Ed.* **2019**, *58*, 2474-2478.
37. Rodríguez-Escrich, C.; Pericàs, M. A. Organocatalysis on Tap: Enantioselective Continuous Flow Processes Mediated by Solid-Supported Chiral Organocatalysts. *Eur. J. Org. Chem.* **2015**, 1173-1188.
38. Rodríguez-Escrich, C.; Pericàs, M. A. Catalytic Enantioselective Flow Processes with Solid-Supported Chiral Catalysts. *Chem. Rec.* **2019**, *19*, 1872-1890.
39. Jas, G.; Kirschning, A. Continuous Flow Techniques in Organic Synthesis. *Chem. Eur. J.* **2003**, *9*, 5708-5723.
40. Kirschning, A.; Jas, G. Applications of Immobilized Catalysts in Continuous Flow Processes. In *Immobilized Catalysts. Topics in Current Chemistry*, Kirschning, A., Ed. Springer: Berlin, Heidelberg, 2004; Vol. 242, pp 209-239.
41. Phan, N. T. S.; Brown, D. H.; Styring, P. A Facile Method for Catalyst Immobilisation on Silica: Nickel-Catalysed Kumada Reactions in Mini-Continuous Flow and Batch Reactors. *Green Chem.* **2004**, *6*, 526-532.
42. Baxendale, I. R.; Deeley, J.; Griffiths-Jones, C. M.; Ley, S. V.; Saaby, S.; Tranmer, G. K. A Flow Process for the Multi-Step Synthesis of the Alkaloid Natural Product Oxomaritidine: a New Paradigm for Molecular Assembly. *Chem. Commun.* **2006**, 2566-2568.
43. Baxendale, I. R.; Griffiths-Jones, C. M.; Ley, S. V.; Tranmer, G. K. Microwave-Assisted Suzuki Coupling Reactions with an Encapsulated Palladium Catalyst for Batch and Continuous-Flow Transformations. *Chem. Eur. J.* **2006**, *12*, 4407-4416.
44. Kirschning, A.; Solodenko, W.; Mennecke, K. Combining Enabling Techniques in Organic Synthesis: Continuous Flow Processes with Heterogenized Catalysts. *Chem. Eur. J.* **2006**, *12*, 5972-5990.
45. Baxendale, I. R.; Ley, S. V.; Mansfield, A. C.; Smith, C. D. Multistep Synthesis Using Modular Flow Reactors: Bestmann-Ohira Reagent for the Formation of Alkynes and Triazoles. *Angew. Chem. Int. Ed.* **2009**, *48*, 4017-4021.
46. Ceylan, S.; Kirschning, A. Organic Synthesis with Mini Flow Reactors Using Immobilised Catalysts. In *Recoverable and Recyclable Catalysts*, Benaglia, M., Ed. Wiley: Chichester, 2009; pp 379-410.
47. Alza, E.; Rodríguez-Escrich, C.; Sayalero, S.; Bastero, A.; Pericàs, M. A., A Solid-Supported Organocatalyst for Highly Stereoselective, Batch, and Continuous-Flow Mannich Reactions. *Chem. Eur. J.* **2009**, *15*, 10167-10172.
48. Bedore, M. W.; Zaborenko, N.; Jensen, K. F.; Jamison, T. F. Aminolysis of Epoxides in a Microreactor System: A Continuous Flow Approach to β -Amino Alcohols. *Organic Process Research & Development* **2010**, *14*, 432-440.
49. Alza, E.; Sayalero, S.; Cambeiro, X. C.; Martín-Rapún, R.; Miranda, P. O.; Pericàs, M. A. Catalytic Batch and Continuous Flow Production of Highly Enantioenriched Cyclohexane Derivatives with Polymer-Supported Diarylprolinol Silyl Ethers. *Synlett* **2011**, 464-468.
50. Wegner, J.; Ceylan, S.; Kirschning, A. Ten Key Issues in Modern Flow Chemistry. *Chem. Commun.* **2011**, *47*, 4583-4592.
51. Ayats, C.; Henseler, A. H.; Pericàs, M. A. A Solid-Supported Organocatalyst for Continuous-Flow Enantioselective Aldol Reactions. *ChemSusChem* **2012**, *5*, 320-325.
52. Fan, X.; Sayalero, S.; Pericàs, M. A., Asymmetric α -Amination of Aldehydes Catalyzed by PS-Diphenylprolinol Silyl Ethers: Remediation of Catalyst Deactivation for Continuous Flow Operation. *Adv. Synth. Cat.* **2012**, *354*, 2971-2976.
53. Kasaplar, P.; Rodríguez-Escrich, C.; Pericàs, M. A. Continuous Flow, Highly Enantioselective Michael Additions Catalyzed by a PS-Supported Squaramide. *Org. Lett.* **2013**, *15*, 3498-3501.
54. Tsubogo, T.; Ishiwata, T.; Kobayashi, S. Asymmetric Carbon-Carbon Bond Formation under Continuous-Flow Conditions with Chiral Heterogeneous Catalysts. *Angew. Chem. Int. Ed.* **2013**, *52*, 6590-6604.
55. Puglisi, A.; Benaglia, M.; Chiroli, V. Stereoselective Organic Reactions Promoted by Immobilized Chiral Catalysts in Continuous Flow Systems. *Green Chem.* **2013**, *15*, 1790-1813.
56. Cañellas, S.; Ayats, C.; Henseler, A. H.; Pericàs, M. A. A Highly Active Polymer-Supported Catalyst for Asymmetric Robinson Annulations in Continuous Flow. *ACS Catal.* **2017**, *7*, 1383-1391.
57. *Chiral Catalyst Immobilization and Recycling*; De Vos, D.; Vankelecom, I. F.; Jacobs, P. A., Eds.; Wiley-VCH: Weinheim, 2000; pp 1-320.
58. Cozzi, F. Immobilization of Organic Catalysts: When, Why, and How. *Adv. Synth. Cat.* **2006**, *348*, 1367-1390.
59. *Handbook of Asymmetric Heterogeneous Catalysis*; Ding, K.; Uozumi, Y., Eds.; Wiley-VCH: Weinheim, 2008; pp 1-448.
60. Gruttadauria, M.; Giacalone, F.; Noto, R. Supported Proline and Proline-Derivatives as Recyclable Organocatalysts. *Chem. Soc. Rev.* **2008**, *37*, 1666-1688.
61. Jimeno, C.; Sayalero, S.; Pericàs, M. A. Covalent Heterogenization of Asymmetric Catalysts on Polymers and Nanoparticles. In *Heterogenized Homogeneous Catalysts for Fine Chemicals Production. Catalysis by Metal Complexes*, Barbato, P.; Liguori, F., Eds. Springer: Dordrecht, 2010; Vol. 33, pp 123-170.
62. Rueping, M.; Sugiono, E.; Steck, A.; Theissmann, T. Synthesis and Application of Polymer-Supported Chiral Brønsted Acid Organocatalysts. *Adv. Synth. Cat.* **2010**, *352*, 281-287.
63. Kundu, D. S.; Schmidt, J.; Bleschke, C.; Thomas, A.; Blechert, S. A Microporous Binol-Derived Phosphoric Acid. *Angew. Chem. Int. Ed.* **2012**, *51*, 5456-5459.
64. Osorio-Planes, L.; Rodríguez-Escrich, C.; Pericàs, M. A. Enantioselective Continuous-Flow Production of 3-Indolylmethanamines Mediated by an Immobilized Phosphoric Acid Catalyst. *Chem. Eur. J.* **2014**, *20*, 2367-2372.
65. Clot-Almenara, L.; Rodríguez-Escrich, C.; Osorio-Planes, L.; Pericàs, M. A. Polystyrene-Supported TRIP: A Highly Recyclable Catalyst for Batch and Flow Enantioselective Allylation of Aldehydes. *ACS Catal.* **2016**, *6*, 7647-7651.
66. Clot-Almenara, L.; Rodríguez-Escrich, C.; Pericàs, M. A., Desymmetrisation of *meso*-Diones Promoted by a Highly Recyclable Polymer-Supported Chiral Phosphoric Acid Catalyst. *RSC Adv.* **2018**, *8*, 6910-6914.
67. Zhang, X.; Kormos, A.; Zhang, J. Self-Supported BINOL-Derived Phosphoric Acid Based on a Chiral Carbazolic Porous Framework. *Org. Lett.* **2017**, *19*, 6072-6075.
68. Cheng, H.-G.; Miguélez, J.; Miyamura, H.; Yoo, W.-J.; Kobayashi, S. Integration of Aerobic Oxidation and Intramolecular Asymmetric Aza-Friedel-Crafts Reactions with a Chiral Bifunctional Heterogeneous Catalyst. *Chem. Sci.* **2017**, *8*, 1356-1359.
69. Shih, J.-L.; Nguyen, T. S.; May, J. A., Organocatalyzed Asymmetric Conjugate Addition of Heteroaryl and Aryl Trifluoroborates: a Synthetic Strategy for Discoipyrrole D. *Angew. Chem., Int. Ed.* **2015**, *54*, 9931-9935.
70. For a related, multiple nucleophilic aromatic substitution involving 2,3,5,6-tetrafluoroterephthalonitrile, see: Weng, X.; Baez, J. E.; Khiterer, M.; Hoe, M. Y.; Bao, Z.; Shea, K. J. Chiral Polymers of Intrinsic Microporosity: Selective Membrane Permeation of Enantiomers. *Angew. Chem. Int. Ed.* **2015**, *54*, 11214-11218.
71. (a) Wuitschik, G.; Rogers-Evans, M.; Mueller, K.; Fischer, H.; Wagner, B.; Schuler, F.; Polonchuk, L.; Carreira, E. M. Oxetanes as Promising Modules in Drug Discovery. *Angew. Chem. Int. Ed.* **2006**, *45*, 7736-7739; (b) Wuitschik, G.; Carreira, E. M.; Wagner, B.; Fischer, H. Parrilla, I.; Schuler, F.; Rogers-Evans, M.; Muller, K. Oxetanes in Drug Discovery: Structural and Synthetic Insights. *J. Med. Chem.* **2010**, *53*, 3227-3246; (c) Burkhard, J. A.; Wuitschik, G.; Rogers-Evans, M.; Mueller, K.; Carreira, E. M. Oxetanes as Versatile Elements in Drug Discovery and Synthesis. *Angew. Chem. Int. Ed.* **2010**, *49*, 9052-9067; (d) Burkhard, J. A.; Wuitschik, G.; Plancher, J.-M.; Rogers-Evans, M.; Carreira, E. M. Synthesis and Stability of Oxetane Analogs of Thalidomide and Lenalidomide. *Org. Lett.* **2013**, *15*, 4312-4315; (e) Moller, G. P.; Muller, S.; Wolfstader, B. T.; Wolftrum, S.; Schepmann, D.; Wunsch, B.; Carreira, E. M. Oxetanyl Amino Acids for Peptidomimetics. *Org. Lett.* **2017**, *19*, 2510-2513; (f) Geary, G. C.; Nortcliffe, A.; Pearce, C. A.; Hamza, D.; Jones, G.; Moody, C. J.

Densely Functionalised Spirocyclic Oxetane-Piperidine Scaffolds for Drug Discovery. *Bioorg. Med. Chem.* **2018**, *26*, 791-797.

72. Wang, Z.; Chen, Z.; Sun, J. Catalytic Enantioselective Intermolecular Desymmetrization of 3-Substituted Oxetanes. *Angew. Chem. Int. Ed.* **2013**, *52*, 6685-6688.

73 (a) Jumde, R. P.; Evangelisti, C.; Mandoli, A.; Scotti, N.; Psaro, R. Aminopropyl-Silica-Supported Cu Nanoparticles: An Efficient Catalyst for Continuous-Flow Huisgen Azide-Alkyne Cycloaddition (CuAAC). *J. Catal.* **2015**, *324*, 25-31; (b) Wen, J.; Wu, K.; Yang, D.; Tian, J.; Huang, Z.; Filatov, A. S.; Lei, A. Lin, X.-M. Low-Pressure Flow Chemistry of CuAAC Click Reaction Catalyzed by Nanoporous AuCu Membrane. *ACS Appl. Mater. Inter.* **2018**, *10*, 25930-25935; (c) Santos de Sa, D.; Bustamante, R. A.; Rocha, C. E. R.; Diniz da Silva, V.; Rodrigues, E. J. R. Muller, C. D. B.; Ghavami, K.; Massi, A.; Pandoli, O. G. Fabrication of Lignocellulose-Based Microreactors: Copper-Functionalized Bamboo for Continuous-Flow CuAAC Click Reactions. *ACS Sust. Chem. Eng.* **2019**, *7*, 3267-3273.

74. (a) Cheong, P. H.-Y.; Legault, C. Y.; Um, J. M.; Çelebi-Ölçüm, N.; Houk, K. N. Quantum Mechanical Investigations of Organocatalysis: Mechanisms, Reactivities, and Selectivities. *Chem. Rev.* **2011**, *111*, 5042-5137; (b) Champagne, A.; Houk, K. N. Origins of Selectivity and General Model for Chiral Phosphoric Acid-Catalyzed Oxetane Desymmetrizations. *J. Am. Chem. Soc.* **2016**, *138*, 12356-12359; (c) Duarte, F.; Patton, R. S. Molecular Recognition in Asymmetric Counteranion Catalysis: Understanding Chiral Phosphate-Mediated Desymmetrization. *J. Am. Chem. Soc.* **2017**, *139*, 8886-8896.

75. Seguin, T. J.; Wheeler, S. E. Competing Noncovalent Interactions Control the Stereoselectivity of Chiral Phosphoric Acid Catalyzed Ring Openings of 3-Substituted Oxetanes. *ACS Catal.* **2016**, *6*, 7222-7228.

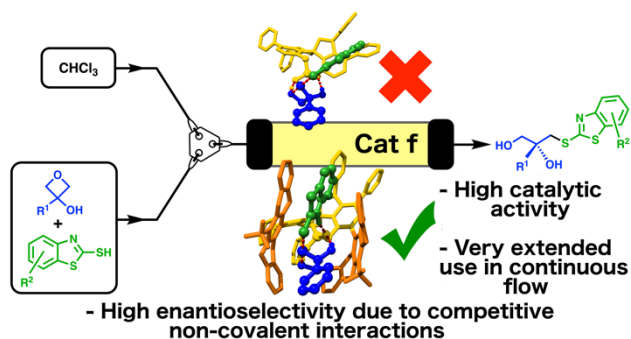
76. Xie, J.-G.; Quan, J.; Li, S.-B.; Zheng, Y.; Zhu, L.-M. SH-Methylation of SH-Containing Heterocycles with Dimethyl Carbonate via Phase-Transfer Catalytic Reaction. *Synth. Commun.* **2011**, *41*, 871-878.

77. Lefebvre, C.; Rubez, G.; Khartabil, H.; Boisson, J.-C.; Contreas-García, J.; Hénon, E. Accurately Extracting the Signature of Intermolecular Interactions Present in the NCI Plot of the Reduced Density Gradient versus Electron Density. *Chem. Phys. Phys. Chem.* **2017**, *17*, 17928-17936.

78. Lu, T.; Chen, F. Multiwfn: A Multifunctional Wavefunction Analyzer. *J. Comput. Chem.* **2012**, *33*, 580-592.

79. It is worth mentioning that 9-anthryl substituents in **Cat a**, one of the catalytic systems also studied by Seguin and Wheeler⁷⁴ are unable and adapt to the substrates by bending while aromatic stabilization remains intact according to the reliable theoretical model used in the present calculations. Accordingly, the 9-anthryl wings in **Cat a** undergo very negligible deviations from planarity throughout the catalytic cycle.

Table of Contents Artwork



Synopsis TOC

SPINOL derivatives containing polymerizable styryl units have been convergently assembled, converted to SPINOL-derived chiral phosphoric acids (SPAs) and immobilized onto cross-linked polystyrene. The optimal immobilized species brings about the catalytic desymmetrization of 3,3-disubstituted oxetanes in up to 90% yield with up to >99% enantioselectivity, exhibiting a very high recyclability and being suitable for extended operation in continuous flow. DFT calculations rationalize the effect on enantioselectivity of bulky, conformationally adaptable substituents at 6,6' on the catalyst structure.
